Activation Free Energy of Nucleation of a Dislocation Pair in Magnesium

AUTHOR(S):

Uranagase, Masayuki; Kamigaki, Sana; Matsumoto, Ryosuke; Miyazaki, Noriyuki

CITATION:

Uranagase, Masayuki ...[et al]. Activation Free Energy of Nucleation of a Dislocation Pair in Magnesium. MATERIALS TRANSACTIONS 2013, 54(5): 680-685

ISSUE DATE:

2013

URL:

http://hdl.handle.net/2433/194078

Materials Transactions, Vol. 54, No. 5 (2013) pp. 680 to 685
Special Issue on Long-Period Stacking Ordered Structure and Its Related Materials (I)

Activation Free Energy of Nucleation of a Dislocation Pair in Magnesium

Masayuki Uranagase, Sana Kamigaki*, Ryosuke Matsumoto and Noriyuki Miyazaki

Department of Mechanical Engineering and Science, Graduate School of Engineering, Kyoto University, Kyoto 606-8501, Japan

Kink deformation is one of the possible principal deformation modes of alloys with a long-period stacking ordered structure under compression parallel to the basal plane. In this deformation, dislocation pairs are massively nucleated, and these dislocations align in a line to form kink bands. In this study, we investigated the nucleation of a dislocation pair in a pure magnesium single crystal by molecular dynamics simulations. We also evaluated the activation free energy of nucleation of a dislocation pair and investigated the dependence of the activation free energy on the applied shear stress and temperature. [doi:10.2320/matertrans.MI201213]

(Received November 16, 2012; Accepted February 22, 2013; Published April 12, 2013)

Keywords: *molecular dynamics simulation, metadynamics method, activation free energy, dislocation nucleation, magnesium*

1. Introduction

Magnesium is lightweight and hence is expected to be used in various industrial products. However, because of its low ductility and formability, the widespread application of magnesium is severely restricted. Moreover, the specific strength of magnesium is slightly inferior to that of aluminum. To overcome these drawbacks of magnesium, various magnesium alloys have been developed.[1] In particular, the recently developed Mg–Zn–RE alloys have excellent strength as well as reasonable ductility.[2] In the last decade, various experiments were performed to investigate nature of these alloys, such as structure[3–7] and mechanical properties.[8–11]

The Mg–Zn–RE alloys have long-period stacking ordered (LPSO) structure, that is, there are face centered cubic (FCC) structured Zn- and RE-rich regions are arranged periodically within the hexagonal close packed (HCP) Mg rich region. This type of structure obstructs the motion of dislocations, thus enhancing the strength of these alloys. To apply these alloys in a variety of applications, the deformation mechanisms must be elucidated. Kink deformation, which was originally suggested to be the main deformation mechanism in cadmium in compression tests,[12] is proposed as the principal deformation mode when the LPSO phases in Mg–Zn–RE alloys are compressed parallel to the basal plane.[9] This is contrary to the case of conventional magnesium alloys, where twinning deformation is dominant. In kink deformation, a nucleated dislocation pair separates into individual dislocations, which then move in opposite direction and this is followed by kinking boundaries formation by aligning dislocations in a line.

In the present study, we focus on the homogeneous nucleation of a dislocation pair in a material as the first step toward understanding kink deformation. For simplicity, we performed atomistic simulations on a pure magnesium single crystal. Although molecular dynamics (MD) simulations can trace the motion of all the atoms in a given system, we could follow the dynamics of the atoms only for a very short time scale, typically for a few nanoseconds. Here, in order to discuss the dislocation behavior on the time scale used in real experiments, we combined MD simulation with the metadynamics method.[13,14]

*Graduate Student, Kyoto University

The rest of this paper is organized as follows. Section 2 introduces a model used in our analysis. The simulation details are explained, including the metadynamics method, which enables us to estimate the activation free energy of nucleation of a dislocation pair. Section 3 is devoted to the analysis of the simulation results. The nucleation of a dislocation pair is shown by the MD simulation in combination with the metadynamics method, and then, the activation free energy of nucleation of a dislocation pair in basal and prismatic slips is calculated. In particular, the dependence of the activation free energy on the temperature and applied shear stress is discussed. Section 4 includes concluding remarks.

2. Model and Methods

In the present work, we perform atomistic simulations on a single crystal of magnesium. The interatomic potential proposed by Sun *et al.*,[15] which is based on the embedded atom method,[16] is used for evaluating the energy and force. This potential gives the lattice constant $a = 0.3184$ nm and the axis ratio $c/a = 1.628$, where c is the length of the c-axis of the HCP lattice. Initially, 32,000 magnesium atoms are placed at the HCP lattice points. The dimensions of the magnesium crystal at room temperature and atmospheric pressure are $80a$, $10\sqrt{3}a$ and $10c$ in the $[11\bar{2}0]$, $[\bar{1}100]$ and $[0001]$ directions, respectively. Region D_0 of the simulation box before starting the simulation is defined by

$$D_0 = [-40a, 40a] \times [-5\sqrt{3}a, 5\sqrt{3}a] \times [-5c, 5c], \quad (1)$$

and the periodic boundary condition is applied in each direction in order to eliminate the effects of free surfaces. The main aim of our simulation is to observe the nucleation of a dislocation pair for various temperature (T) and shear stress (τ) values under the condition that the hydrostatic pressure is zero. T and τ are kept constant by applying the Nóse-Hoover method[17,18] and Parrinello–Rahman method,[19,20] respectively. The shape of the simulation box changes with time so that the designated level of stress is maintained. Magnesium is equilibrated at temperature T and zero hydrostatic pressure before applying the shear stress τ in the slip direction on the plane parallel to the slip plane.

In the conventional MD simulation, the dynamics of atoms can be traced only for a few nanoseconds, which is too short

to study a given phenomenon in real experiments. To overcome this problem, we combine our MD simulation with the metadynamics method. In this method, we consider collective variables and accelerate the dynamics of these variables by adding the bias potential V_b, which urges the system to escape from the (meta) stable state. The advantage of this method is that by choosing the appropriate collective variables, one can estimated the activation free energies of various phenomena from the accumulated bias potential. It is necessary to choose collective variables carefully, because any inappropriate choice may result in unwanted behavior. We consider two regions D_u and D_l, which are included in D_0, in the plane just above and below the site of nucleation of a dislocation pair, respectively. Then, we define X by

$$X = \sum_i r_{i,\alpha}\left[\frac{1_{D_u}(\boldsymbol{r}_i^0)}{N_u} - \frac{1_{D_l}(\boldsymbol{r}_i^0)}{N_l}\right], \tag{2}$$

where α represents the slip direction, $\boldsymbol{r}_i$ is the position of atom i, $\boldsymbol{r}_i^0$ is the initial value of $\boldsymbol{r}_i$, and $r_{i,\alpha}$ is the α component of $\boldsymbol{r}_i$. $1_D(\boldsymbol{r})$ is an indicator function, which is defined by

$$1_D(\boldsymbol{r}) = \begin{cases} 1 & \boldsymbol{r} \in D \\ 0 & \boldsymbol{r} \notin D \end{cases} \tag{3}$$

and N_u and N_l are given by

$$N_u = \sum_i 1_{D_u}(\boldsymbol{r}_i^0), \quad N_l = \sum_i 1_{D_l}(\boldsymbol{r}_i^0). \tag{4}$$

X corresponds to the distance in the slip direction between the center of mass of the atoms whose reference positions are in D_u and that in D_l. We adopt X as a collective variable for the metadynamics method in this analysis.

The following Gaussian potential is added to the system after every designated number n_{add} of MD steps so that the system escapes from the (meta) stable state:

$$V_G(X;k) = h\exp\left[-\frac{(X - \hat{X}(kn_{add}))^2}{2\delta s^2}\right] \quad (k = 1, 2, \ldots), \tag{5}$$

where kn_{add} is the number of MD steps, henceforth k referred to as metastep, $\hat{X}(kn_{add})$ is value of eq. (2) at kn_{add} MD steps, and h and δs^2 are the height and variance of the Gaussian, respectively, which are tunable parameters in the metadynamics method. Hence, the bias potential at n MD steps is given by

$$V_b(X;n) = \sum_{k=1}^{k_{max}(n)} V_G(X;k), \tag{6}$$

where $k_{max}(n)$ is the maximum integer less than n/n_{add}.

3. Results

First, the time evolution of $\hat{X}$ for $T = 300\,\mathrm{K}$ and $\tau = 700\,\mathrm{MPa}$ is shown in Fig. 1. The shear stress is applied in the $[11\bar{2}0]$ direction on the plane parallel to the (0001) plane. Here, regions D_u and D_l are chosen as the following rectangular box regions:

$$D_u = [-2a, 2a] \times [-5\sqrt{3}a, 5\sqrt{3}a] \times [0, 0.5c],$$
$$D_l = [-2a, 2a] \times [-5\sqrt{3}a, 5\sqrt{3}a] \times [-0.5c, 0]. \tag{7}$$

These D_u and D_l give $N_u = N_l = 80$. If there is no additional potential, $\hat{X}$ stays near 0 nm, with small fluctuations.

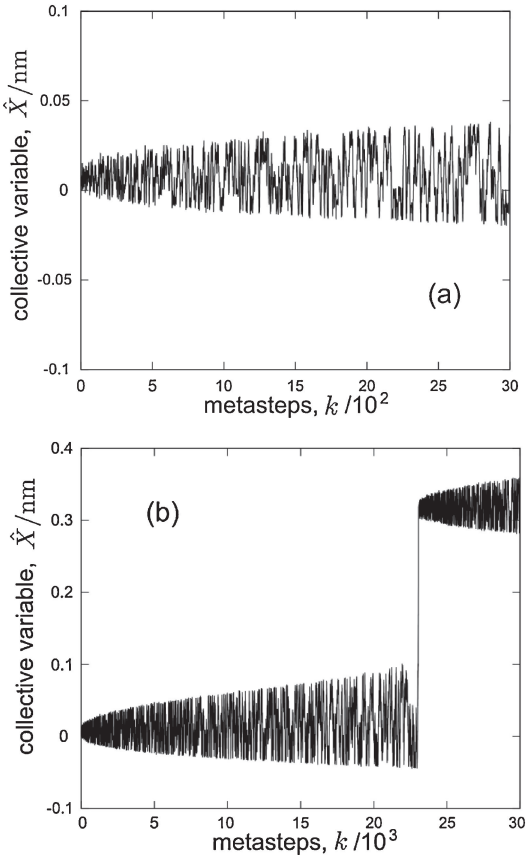

Fig. 1 Time evolution of the collective variable X for $T = 300\,\mathrm{K}$ and $\tau = 700\,\mathrm{MPa}$ on a short time scale (a) and on a long time scale (b).

However, the fluctuation of $\hat{X}$ increases with time because additional potentials urge the system to escape from the stable state. Then, $\hat{X}$ jumps to around 0.3 nm and again $\hat{X}$ fluctuates with increasing amplitude of fluctuation. This implies the existence of stable states at $\hat{X} \simeq 0\,\mathrm{nm}$ and $\hat{X} \simeq 0.3\,\mathrm{nm}$ and a free energy barrier between these stable states. The difference between the values of $\hat{X}$ at two stable states is approximately equal to the distance between the nearest neighbor atoms of magnesium. Therefore, from the time evolution of $\hat{X}$, one can predict the occurrence of a basal slip.

To observe the occurrence of the slip more clearly, we recorded some snapshots of the atoms on the plane above the slip plane for $T = 300\,\mathrm{K}$ and $\tau = 700\,\mathrm{MPa}$, as shown in Fig. 2. In these snapshots, the local structure is evaluated by the common neighbor analysis method.[21] According to this method, atoms are classified into three types, HCP, FCC, or others. First, the atoms are almost regularly placed and slightly disturbed by thermal fluctuation (Fig. 2(a)). When a sufficient bias potential is added, a pair of Shockley partial dislocations with Burgers vectors of $1/3[01\bar{1}0]$ and $-1/3[01\bar{1}0]$, is nucleated, and the atoms located between the two partial dislocations give rise to stacking fault (Fig. 2(b)). With continuous addition of the bias potential, these dislocations move away from each other, and nucleation of a new pair of Shockley partial dislocations whose Burgers vectors are $1/3[10\bar{1}0]$ and $-1/3[10\bar{1}0]$ occurs (Fig. 2(c)). When nucleation of a pair of Shockley partial dislocations occurs twice, a pair of extended dislocations consisting of

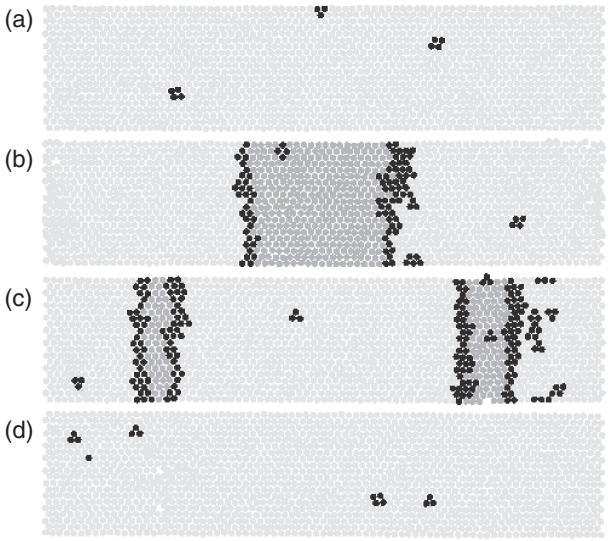

Fig. 2 Snapshots of atoms right above the slip plane for $T = 300$ K and $\tau = 700$ MPa at 21000 (a), 22500 (b), 22700 (c) and 23000 (d) metasteps. Light gray, dark gray and black circles represent HCP, FCC and other structures, respectively.

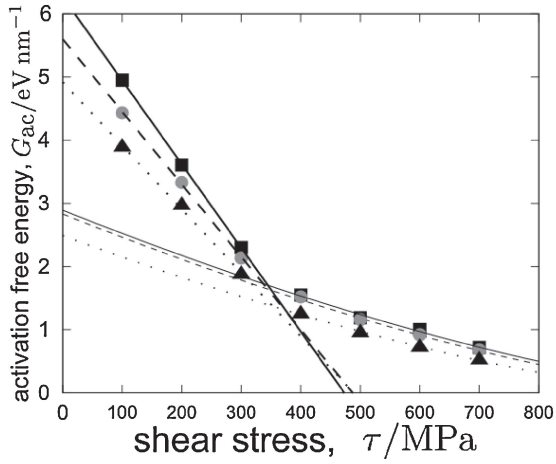

Fig. 3 Activation free energy as a function of applied shear stress τ for temperature $T = 100$ (square), 300 (circle) and 500 K (triangle), respectively. Results of fitting by eq. (17) at $\tau \leq 300$ MPa (thick lines) and $\tau > 300$ MPa (thin curves) for $T = 100$ (solid), 300 (dashed) and 500 K (dotted) are also shown.

two partial dislocations and stacking fault is nucleated. These extended dislocations have Burgers vectors of $1/3[11\bar{2}0]$ and $-1/3[11\bar{2}0]$. Finally, the two extended dislocations annihilate by colliding with each other via the periodic boundary (Fig. 2(d)).

Next, we study the dependence of the activation free energy G_{ac} of nucleation of an extended dislocation pair in the basal slip on the temperature and applied shear stress. Here, shear stress is applied in the $[11\bar{2}0]$ direction on the plane parallel to (0001) plane. Activation free energies of nucleation of a dislocation pair in the basal slip are shown as functions of the applied shear stress for several temperatures in Fig. 3. For every case, D_u and D_l are given by eq. (7). Since the activation free energy is proportional to the length of a dislocation pair, in this work, we define G_{ac} as the activation free energy per nanometer. Hence, the unit of G_{ac} is eV/nm. The activation free energy monotonically decreases as the temperature and/or the applied shear stress increase, though, at high τ the difference between activation free energies for 100 and 300 K becomes very small.

We evaluated the Gibbs free energy by the metadynamics method because we performed simulations at a constant temperature and applied shear stress. The Gibbs free energy of this system is given as a function of T, τ and X. Then, the activation free energy is written as

$$G_{ac}(T,\tau) = G[T,\tau,X_t] - G[T,\tau,X_0], \tag{8}$$

where $G[T, \tau, X]$ signifies that the Gibbs free energy is a complete thermodynamic function of T, τ and X; X_t and X_0 are the values of X at which $G[T, \tau, X]$ becomes the local maximum and local minimum in the X direction, respectively. Accordingly, X_t and X_0 are functions of T and τ.

In order to enable a more meaningful discussion from our discrete data, we consider a method for the interpolation and extrapolation of data. By differentiating eq. (8) with respect to τ, we obtain

$$\begin{aligned}\frac{\partial G_{ac}(T,\tau)}{\partial\tau} &= \left.\frac{\partial G[T,\tau,X]}{\partial\tau}\right|_{X=X_t} - \left.\frac{\partial G[T,\tau,X]}{\partial\tau}\right|_{X=X_0} \\ &\quad + \frac{\partial X_t(T,\tau)}{\partial\tau}\left.\frac{\partial G[T,\tau,X]}{\partial X}\right|_{X=X_t} \\ &\quad - \frac{\partial X_0(T,\tau)}{\partial\tau}\left.\frac{\partial G[T,\tau,X]}{\partial X}\right|_{X=X_0} \\ &= -V(\gamma(T,\tau,X_t) - \gamma(T,\tau,X_0)),\end{aligned} \tag{9}$$

where V is the volume of the system before deformation and $\gamma(T, \tau, X)$ is the strain. Terms including the differentiation with respect to X in eq. (9) vanish because of the extreme value condition.

For $\tau \simeq 0$, eq. (9) is expanded in τ as

$$\begin{aligned}\frac{\partial G_{ac}(T,\tau)}{\partial\tau} &= -V(\gamma(T,0,X_t) - \gamma(T,0,X_0)) \\ &\quad - V\tau\left(\left.\frac{\partial\gamma(T,\tau,X_t)}{\partial\tau}\right|_{\tau=0} - \left.\frac{\partial\gamma(T,\tau,X_0)}{\partial\tau}\right|_{\tau=0}\right) \\ &\quad + O(\tau^2),\end{aligned} \tag{10}$$

and, G_{ac} is expressed up to the linear term as

$$G_{ac}(T,\tau) \simeq G_{ac}(T,0) - \tau V\gamma(T,0,X_t), \tag{11}$$

where the relation $\gamma(T, 0, X_0) = 0$ is used. This linear relation is held in a relatively wide range in τ if the dependence of $\partial\gamma(T, \tau, X)/\partial\tau|_{\tau=0}$ on X can be neglected. Although it is not clear whether the assumption of this dependence is valid for our case, our results, as see below, show linear decrease in the activation free energy with τ at low τ.

To obtain an expression for G_{ac} at high τ, we integrate eq. (9):

$$\begin{aligned}G_{ac}(T,\tau) &= G_{ac}(T,\tau_0) + \int_{\tau_0}^{\tau}\left.\frac{\partial G_{ac}(T,\tau)}{\partial\tau}\right|_{\tau=\tilde{\tau}}\mathrm{d}\tilde{\tau} \\ &= G_{ac}(T,\tau_0) - V\int_{\tau_0}^{\tau}[\gamma(T,\tilde{\tau},X_t) - \gamma(T,\tilde{\tau},X_0)]\mathrm{d}\tilde{\tau},\end{aligned} \tag{12}$$

where τ_0 is the applied stress in the reference state. Generally, strain γ produces an opposing stress τ' in the system. Cahn and Nabarro[22] assumed the following relationship:

$$\tau' = \tau_{ath} - C(\gamma_{ath} - \gamma)^2, \tag{13}$$

Table 1 List of fitting parameters for basal slip.

Temperature (K)	100	300	500
A^{L} (eV/nm)	6.27	5.60	5.40
$\tau^{\mathrm{L}}_{\mathrm{ath}}$ (MPa)	473.2	487.2	455.5
A^{H} (eV/nm)	2.89	2.83	2.49
$\tau^{\mathrm{H}}_{\mathrm{ath}}$ (MPa)	1160	1132	1074

where τ_{ath} is the maximum value of τ' and γ_{ath} is the strain that produces the maximum opposing stress τ_{ath}. Note that this approximation becomes suitable for $\tau' \lesssim \tau_{\mathrm{ath}}$.

X_0 and X_{t} are the values of X in the stable and unstable equilibrium state, respectively. Hence, γ in each state can be determined by the stress balance $\tau = \tau'$. By taking into account the stability, we obtain

$$\gamma(T, \tau, X_0) = \gamma_{\mathrm{ath}} - \sqrt{\frac{\tau_{\mathrm{ath}} - \tau}{C}}, \tag{14}$$

$$\gamma(T, \tau, X_{\mathrm{t}}) = \gamma_{\mathrm{ath}} + \sqrt{\frac{\tau_{\mathrm{ath}} - \tau}{C}}. \tag{15}$$

When $\tau = \tau_{\mathrm{ath}}$, $\gamma(T, \tau, X_0) = \gamma(T, \tau, X_{\mathrm{t}})$. This means that there is no activation process when $\tau = \tau_{\mathrm{ath}}$, that is, $G_{\mathrm{ac}}(T, \tau_{\mathrm{ath}}) = 0$. Finally, by substituting eqs. (14) and (15) in eq. (12) and integrating eq. (12), adopting τ_{ath} as τ_0, G_{ac} is obtained as

$$G_{\mathrm{ac}}(T, \tau) = \frac{4V}{3C^{1/2}}(\tau_{\mathrm{ath}} - \tau)^{3/2}. \tag{16}$$

Here, we adopt the approach proposed by Cahn and Nabarro[22] to obtain $G_{\mathrm{ac}} \propto (\tau_{\mathrm{ath}} - \tau)^{3/2}$ at high τ, but even a different approach can lead to this relationship.[23]

From the above discussion, we try to fit the following equation to our data:

$$G_{\mathrm{ac}}(T, \tau) = A\left(1 - \frac{\tau}{\tau_{\mathrm{ath}}}\right)^{\alpha}, \tag{17}$$

where A is a coefficient independent of τ. Exponent α is set to 1 for $\tau \leq 300$ MPa, while α is set to 3/2 for $\tau \geq 400$ MPa. Therefore, there are two adjustable parameters, τ_{ath} and A, in eq. (17). In Fig. 3, the fitting results are shown as curves. The values of the parameters used in the fitting are listed in Table 1.

The activation free energy is related to the frequency f_{n} of nucleation by

$$f_{\mathrm{n}} = \nu \exp\left(-\frac{G_{\mathrm{ac}}}{k_{\mathrm{B}}T}\right), \tag{18}$$

where k_{B} is the Boltzmann constant and ν is a coefficient corresponding to the number of trials to pass through the barrier. Typically, nucleation can occur on the usual experimental time scale when $G_{\mathrm{ac}} = 25 \sim 35\, k_{\mathrm{B}}T$. If we take $G_{\mathrm{ac}} = 30\, k_{\mathrm{B}}T$, which becomes 0.75~0.78 eV at room temperature, as the criterion for nucleation in real experiments, from the fitting functions, the shear stress required for the nucleation of a dislocation pair whose length is 1 nm becomes 928, 654 and 380 MPa for $T = 100$, 300 and 500 K, respectively. For the nucleation of a dislocation pair whose length is 10 nm, it is necessary to apply a shear stress $\tau = 1110$, 1029 and 924 MPa for $T = 100$, 300 and 500 K, respectively. These stresses are much higher as compared to the critical resolved shear stress for the basal slip of the magnesium single crystal, which is about a few mega Pascals.[24]

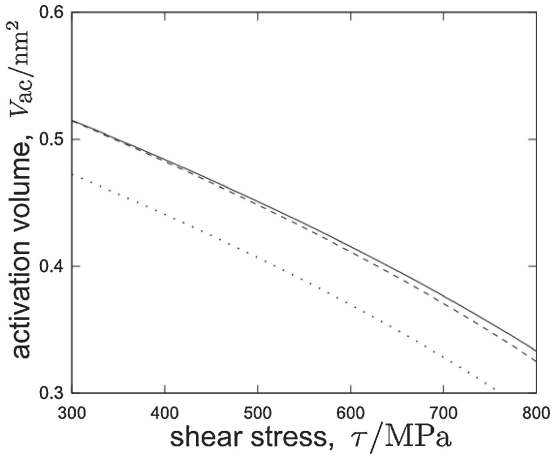

Fig. 4 Activation volume calculated from eq. (19) for temperature $T = 100$ (solid), 300 (dashed) and 500 K (dotted), respectively.

In the case of kink deformation, when LPSO structures are compressed nearly parallel to the basal plane and failure by kinking occurs, the structures usually show very high yield stress of several hundred mega Pascals. Hence, the resolved shear stress in the basal slip direction is much lower than the values discussed in the previous paragraph. This result suggests that some kind of dislocation source is required for kink deformation. Furthermore, it is noteworthy that a dislocation source is required in each basal plane because kink deformation is believed to be caused through massive nucleations of dislocation pairs on different planes.

From the functions fitted to our simulation data, the activation volume $V_{\mathrm{ac}} \equiv -\partial G_{\mathrm{ac}}(T, \tau)/\partial\tau$ of nucleation can be calculated as

$$V_{\mathrm{ac}} = \begin{cases} A^L/\tau^L_{\mathrm{ath}} & \text{for low } \tau \\ 3A^H(1 - (\tau/\tau^H_{\mathrm{ath}}))^{1/2}/2\tau^H_{\mathrm{ath}} & \text{for high } \tau \end{cases}, \tag{19}$$

where $A^{\mathrm{L}}(A^{\mathrm{H}})$ and $\tau^{\mathrm{L}}_{\mathrm{ath}}(\tau^{\mathrm{H}}_{\mathrm{ath}})$ are the parameters used for the fitting at low (high) τ. V_{ac} enables us to quantify the volume of the region that includes the atoms contributing to this nucleation. V_{ac} at low τ becomes 2.12, 1.84 and 1.61 nm^2 for $T = 100$, 300 and 500 K, respectively. Here, since G_{ac} is defined as the activation free energy per nanometer, the unit of activation volume is nm^2. The V_{ac} values calculated from eq. (19) are plotted in Fig. 4. V_{ac}, too, monotonically decreases as the applied shear stress is increased. When the atomic volume is denoted by v, V_{ac}/v, which is the number of atoms involved in the collective motion for activation, becomes about 100 and 20 at $\tau = 100$ and 700 MPa, respectively.

Although nucleation of a dislocation pair in the basal slip contributes to kink deformation, it is interesting to study the nucleation in the case of other slips as well for comparison. The results obtained for the prismatic slip are shown in Fig. 5. In this case, the shear stress is applied in the $[11\bar{2}0]$ direction on the plane parallel to $(1\bar{1}00)$. D_{u} and D_{l} are chosen as

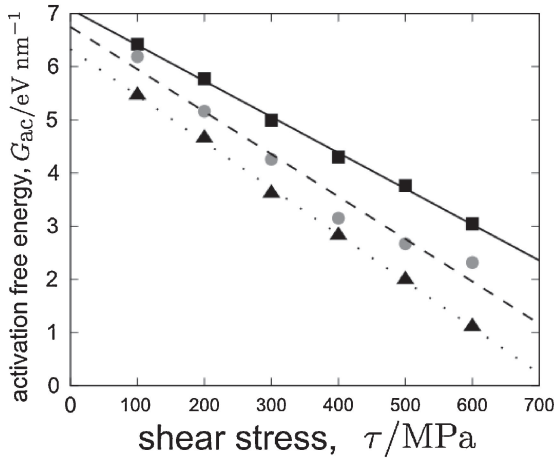

Fig. 5 Activation free energy as a function of applied shear stress τ for temperature $T = 100$ (square), 300 (circle) and 500 K (triangle), respectively. Solid, dashed and dotted lines are results of linear fitting for $T = 100$, 300 and 500 K, respectively.

Table 2 List of fitting parameters for prismatic slip.

Temperature (K)	100	300	500
A^{L} (eV/nm)	7.08	6.75	6.33
τ^{L}_{ath} (MPa)	1049	845.6	726.1

$$D_u = [-15a, 15a] \times [0, \sqrt{3}a/2] \times [-5c, 5c],$$
$$D_l = [-15a, 15a] \times [-\sqrt{3}a/2, 0] \times [-5c, 5c], \quad (20)$$

if $\tau \leq 300$ MPa and

$$D_u = [-10a, 10a] \times [0, \sqrt{3}a/2] \times [-5c, 5c],$$
$$D_l = [-10a, 10a] \times [-\sqrt{3}a/2, 0] \times [-5c, 5c], \quad (21)$$

if $\tau > 300$ MPa. We note that the activation free energies evaluated by the metadynamics method are not strongly dependent on choice of D_u and D_l if the prismatic slip is successfully generated. Similar to the case of a basal slip, the activation free energy monotonically decreases as the temperature and/or the applied shear stress increase. From Figs. 3 and 5, we can see that the activation free energy of the prismatic slip is higher than that of the basal slip for the same temperature and applied shear stress.

The activation free energy changes almost linearly within the stress range we studied. This is in contrast to the case of the basal slip, where a linear dependence of the activation free energy on stress in the low stress range is seen only for $\tau \leq 300$ MPa. Here, the activation free energy obtained from MD simulation is fitted only by a linear equation. The lines in Fig. 5 are the results of fitting; the parameters used for the fitting are listed in Table 2.

From Figs. 3 and 5, we can see that the slope of the activation free energy becomes more gradual as compared to the case of the basal slip. One of the reasons of this may be attributed to the difference between two components C_{44} and C_{66} of the anisotropic elastic constant tensor. C_{44} and C_{66} contributes to the strain due to the shear stress applied in the $[11\bar{2}0]$ direction on the plane parallel to the (0001) plane and parallel to the $(1\bar{1}00)$ plane, respectively. The interatomic potential used in our simulations gives $C_{44} = 12.8$ GPa and $C_{66} = (C_{11} - C_{12})/2 = 22.2$ GPa.[15] Hence, if the shear stresses with the same magnitude are applied in the $[11\bar{2}0]$ direction, the strain due to the shear stress on the basal plane is larger than that on the prismatic plane. As shown in eq. (11), the absolute value of the slope of the activation free energy, which also affects the region where the linear approximation becomes valid, increases as the strain of the system increases.

Although the activation free energy for the nucleation of prismatic dislocation pairs is higher than that for the basal dislocation pairs under the same resolved shear stress, prismatic slip may preferentially occur under compressive deformation parallel to the basal plane. Interfaces such as grain boundaries and free surfaces and stress concentration may reduce the resolved shear stress required for the nucleation of prismatic dislocation to a few ten percents and the value become compatible to experimental data of yield stress of LPSO structured crystals. Non-basal slips prior to basal slips may induce kink deformation, as indicated by MD simulations.[25]

4. Conclusion

We investigated the dislocation nucleation processes in pure magnesium single crystal via MD simulation combined with the metadynamics method. We showed that basal and prismatic slips are successfully reproduced by the metadynamics method when collective variables are appropriately chosen. In particular, we focused on the activation free energy of nucleation, which can be estimated by this method. The activation free energy monotonically decreases with an increase in temperature and/or applied shear stress. Moreover, the activation free energy of the basal slip is lower than that of the prismatic slip, for the same temperature and applied shear stress.

From the simulation data, we estimated the shear stresses required to generate a dislocation pair. These stresses are much higher as compared to the critical resolved shear stress of magnesium alloys with LPSO phases. This implies that some dislocation sources such as other pinned dislocations are required for kink deformation in LPSO phases. For verifying the validity of kink deformation, it is important to analyze the activation free energy of nucleation of a dislocation pair from some sources. We plan to study this problem in detail in the near future.

Acknowledgements

This work was supported by a Grant-in-Aid for Scientific Research on Innovative Areas “Synchronized Long-Period Stacking Ordered Structure” from the Ministry of Education, Culture, Sports, Science and Technology (MEXT) of Japan.

REFERENCES

1) S. R. Agnew and J. F. Nie: Scr. Mater. **63** (2010) 671–673.
2) Y. Kawamura, K. Hayashi, A. Inoue and T. Masumoto: Mater. Trans. **42** (2001) 1172–1176.
3) E. Abe, Y. Kawamura, K. Hayashi and A. Inoue: Acta Mater. **50** (2002) 3845–3857.
4) T. Itoi, T. Seimiya, Y. Kawamura and M. Hirohashi: Scr. Mater. **51**

(2004) 107–111.
5) M. Matsuda, S. Ii, Y. Kawamura, Y. Ikuhara and M. Nishida: Mater. Sci. Eng. A **393** (2005) 269–274.
6) D. Egusa and E. Abe: Acta Mater. **60** (2012) 166–178.
7) Y. M. Zhu, A. J. Morton and J. F. Nie: Acta Mater. **60** (2012) 6562–6572.
8) M. Yamasaki, T. Anan, S. Yoshimoto and Y. Kawamura: Scr. Mater. **53** (2005) 799–803.
9) K. Hagihara, N. Yokotani and Y. Umakoshi: Intermetallics **18** (2010) 267–276.
10) X. H. Shao, Z. Q. Yang and X. L. Ma: Acta Mater. **58** (2010) 4760–4771.
11) S. Miura, S. Imagawa, T. Toyoda, K. Ohkubo and T. Mohri: Mater. Trans. **49** (2008) 952–956.
12) E. Orowan: Nature **149** (1942) 643–644.
13) A. Laio and M. Parrinello: Proc. Natl. Acad. Sci. U.S.A. **99** (2002) 12562–12566.
14) A. Laio and F. L. Gervasio: Rep. Prog. Phys. **71** (2008) 126601.
15) D. Y. Sun, M. I. Mendelev, C. A. Becker, K. Kudin, T. Haxhimali, M. Asta, J. J. Hoyt, A. Karma and D. J. Srolovitz: Phys. Rev. B **73** (2006) 024116.
16) M. S. Daw and M. I. Baskes: Phys. Rev. B **29** (1984) 6443–6453.
17) S. Nosé: J. Chem. Phys. **81** (1984) 511–519.
18) W. G. Hoover: Phys. Rev. A **31** (1985) 1695–1697.
19) M. Parrinello and A. Rahman: J. Appl. Phys. **52** (1981) 7182–7190.
20) J. R. Ray and A. Rahman: J. Chem. Phys. **80** (1984) 4423–4428.
21) J. D. Honeycutt and H. C. Andersen: J. Phys. Chem. **91** (1987) 4950–4963.
22) J. W. Cahn and F. R. N. Nabarro: Philos. Mag. A **81** (2001) 1409–1426.
23) A. H. Cottrell: Philos. Mag. Lett. **82** (2002) 65–70.
24) A. Chapuis and J. H. Driver: Acta Mater. **59** (2011) 1986–1994.
25) R. Matsumoto, M. Uranagase and N. Miyazaki: Mater. Trans. **54** (2013) doi:10.2320/matertrans.MI201211.